Available online at www.sciencedirect.com
ScienceDirect
Journal of Sound and Vibration 302 (2007) 643–656
JOURNAL OF SOUND AND VIBRATION
www.elsevier.com/locate/jsvi

Chaotic attitude maneuvers in spacecraft with a completely liquid-filled cavity

Yue Baozeng*, Xie Jiafang

Department of Mechanics, School of Science, Beijing Institute of Technology, Beijing 100081, China

Received 6 September 2005; received in revised form 7 November 2006; accepted 13 November 2006
Available online 20 February 2007

Abstract

This paper investigates the problem of chaotic dynamics in attitude transition maneuvers. We consider the case of a rigid body with a completely liquid-filled cavity, whose spin changes from the minor axis to the major axis under the influence of viscous damping and low-amplitude oscillating perturbations expressed as external torques. The Melnikov integral is used to predict transversal intersections of the perturbed system's stable and unstable manifolds. After discussing the phase space of the system, the equations of motion are transformed into a form more suitable for the application of Melnikov's method. Melnikov's method yields an analytical criterion for homoclinic chaos, in the form of an inequality written in terms of the system parameters. In addition, the prediction of the Melnikov criterion is compared to numerical simulations of the system. Finally, we investigate the dependence of chaotic dynamics on quantities such as body shape, degree of damping, and frequency of the perturbing torques.

1. Introduction

The attitude evolution of a rigid body under various external torques has been extensively studied over the past few decades, because of this problem's great importance in the field of aerospace engineering. The prediction and control of attitude evolution are important problems in the dynamics of modern spacecraft. It is well known that for a torque-free rigid body with three distinct moments of inertia, rotation is stable about the axes of maximum and minimum moments of inertia but unstable about the third axis. The stable rotations are central points of equilibrium, and the unstable rotation is a saddle point of equilibrium (or 'saddle', for short). When a rigid body is subjected to a small torque, the heteroclinic orbits (separatrices) that connect points of equilibrium are expected to break and perhaps intersect transversally. The existence of transverse intersections between heteroclinic and/or homoclinic orbits implies complex dynamic behavior, in the sense of the Smale horseshoe map, and is one of the necessary conditions for chaotic motion to occur. There is an analytical technique called Melnikov's method that can detect transverse intersections of heteroclinic (homoclinic) orbits and chaotic motion in nonlinear dynamic systems, using ideas that go back to Poincaré. It is often important to accurately predict the timing or sequence of attitude maneuvers, but the presence of

*Corresponding author. Tel.: +86 010 81715812.
E-mail address: bzyue@sohu.com (Y. Baozeng).

0022-460X/$ - see front matter © 2007 Elsevier Ltd. All rights reserved.
doi:10.1016/j.jsv.2006.11.035

chaotic dynamics could render any attempt at prediction useless. It is thus necessary to understand the conditions under which chaos plays a role in the attitude dynamics of any given spacecraft. The equations of motion describing the attitude dynamics of complex, non-rigid spacecraft are readily derived, but analytical solutions have proven elusive. In fact, if the system is nonlinear and thus potentially chaotic, such solutions are fundamentally unobtainable. While numerical solutions to these highly nonlinear equations can be obtained for specific parameter values, many interesting features of the dynamical system can become obscured by this approach. Fortunately, a great deal of physical insight into the behavior of complex systems can be obtained by analyzing the case of a simpler rigid body. A perturbation approach can then be used to model and analyze similar spacecraft, at least in approximation.

Certain dynamical aspects of attitude transition maneuvers have been studied for a special class of spacecraft: the so-called dual-spin satellites. These satellites are reoriented by spinning up rotors relative to the main spacecraft body. Attitude resonances, which may occur during either spin-up or spin-down, have been investigated for this maneuver using perturbation techniques and numerical simulations [1–5]. In the case of single-body satellites, the problem of controlling the final orientation of the major axis has been studied by many authors, such as Barba et al. [6]. The problem of a rigid body with liquid-filled cavities has also been of major concern to aerospace engineers. Rumyantsev has reviewed the problem of stable rigid body motion for fluid-filled bodies [7]; indeed, the Lyapunov–Rumyantsev theorem has found wide application in the design of artificial satellites and liquid-filled projectiles. Rahn has modeled a spacecraft as a rigid body with a spherical, dissipative fuel slug, and found a control system that could guarantee any final orientation after the spin transition [8]. More recently, Gray et al. have used Melnikov's method to detect the presence of chaotic dynamics originating from the saddles of damped satellites. The satellites were subject to small perturbations during an attitude transition maneuver, due to the presence of oscillating sub-masses, a flexible appendage limited to torsional vibrations, and a rotor immersed in a viscous fluid [9,10]. This study used spherical coordinates to transform the equations of motion into a form better suited to Melnikov's method, and was able to derive analytical criteria for the occurrence of chaotic motion in terms of system parameters.

In other recent works, Tong and Tabarrok have used Melnikov's method to investigate the attitude dynamics of self-excited rigid bodies, subject to small perturbation torques in a viscous medium [11]. Cooper and Bishop have used Melnikov's method to study the chaotic attitude dynamics of a rigid body driven by sinusoidally varying torques [12]. Meehan and Asokanthan have studied chaotic motion in a rotating body subject to a sinusoidally varying external torques, with a circumferential nutation damper [13,14]. Using time histories, phase space analysis, Poincaré maps, Lyapunov exponents, and bifurcation diagrams, they investigated the onset of chaos over a range of driving torque amplitudes and frequencies to better understand the effect of control strategies on chaotic systems. For the case of a rigid body subject to small conservative torques, Homes and Marsden have extended Melnikov's method to systems with a topologically nontrivial phase space [15]. They used this version of Melnikov's method to investigate the chaotic motions of a rigid body in a gravitational field, attached to a flywheel and an asymmetric gyrostat.

The goal of this paper is to develop an attitude transition maneuver capable of taking a completely liquid-filled satellites from minor axis to major axis spin while under the influence of low-level damping and non-Hamiltonian, time-periodic perturbations. First, Melnikov's method is employed to investigate the nonlinear attitude motion of a rigid body with a completely liquid-filled cavity. More precisely, Melnikov's method is used to predict the transverse intersections of stable and unstable manifolds for the perturbed rigid body just described. It is shown that there exist transversal intersections of heteroclinic orbits only for certain parameter ranges. Thus, in some cases the motion of a rigid body with a completely liquid-filled cavity subject to small periodic torques could become quite complex, and even give rise to chaotic motion. This type of problem is not only of theoretical interest, but also of great practical importance in satellite design. The criterion obtained here should be of great help in designing spinning satellites, for example. In Section 2, we develop the mathematical equations and derive the appropriate Melnikov function using residue theory. This aspect of the paper is described more fully in the Appendix A. In Section 3, we obtain the existence condition for homoclinic chaos and investigate the dependence of chaotic dynamics on system parameters. In Section 4, we turn to a numerical study of the chaotic attractors. In Section 5, we summarize our results.

2. Mathematical formulation

2.1. Model equations

The spacecraft model considered (Fig. 1) is composed of a rigid carrier body with a completely liquid-filled spherical container. Let x, y, z denote an orthogonal, body-fixed coordinate system aligned with the principal axes of the carrier body, whose origin is at the center of mass c. The rigid body has three angular momentum components H_1, H_2, H_3 defined about the major, intermediate, and minor body axes, respectively. The fuel in the container is modeled as a spherical slug of inertia J surrounded by a viscous layer. Designating the relative angular rates between the spacecraft body and the fuel slug as σ_1, σ_2, σ_3, the equations of motion are

$$\dot{H}_1 = \frac{I_2 - I_3}{(I_3 - J)(I_2 - J)} H_3 H_2 + \mu\sigma_1 + M_1, \tag{1a}$$

$$\dot{H}_2 = \frac{I_3 - I_1}{(I_1 - J)(I_3 - J)} H_1 H_3 + \mu\sigma_2 + M_2, \tag{1b}$$

$$\dot{H}_3 = \frac{I_1 - I_2}{(I_1 - J)(I_2 - J)} H_1 H_2 + \mu\sigma_3 + M_3, \tag{1c}$$

$$\dot{\sigma}_1 = \frac{H_3}{I_3 - J}\sigma_2 - \frac{H_2}{I_2 - J}\sigma_3 - \frac{\dot{H}_1}{I_1 - J} - \frac{\mu\sigma_1}{J}, \tag{1d}$$

$$\dot{\sigma}_2 = \frac{H_1}{I_1 - J}\sigma_3 - \frac{H_3}{I_3 - J}\sigma_1 - \frac{\dot{H}_2}{I_2 - J} - \frac{\mu\sigma_2}{J}, \tag{1e}$$

$$\dot{\sigma}_3 = \frac{H_2}{I_2 - J}\sigma_1 - \frac{H_1}{I_1 - J}\sigma_2 - \frac{\dot{H}_3}{I_3 - J} - \frac{\mu\sigma_3}{J}, \tag{1f}$$

where μ is the viscous damping coefficient of the slug; I_1, I_2, and I_3 are the principal moments of inertia of the spacecraft, including the slug; and M_1, M_2, M_3 are small perturbation torques about the principal axes. The non-Hamiltonian perturbations studied in this work are explicit functions of time, resulting in equations of motion with time-dependent coefficients. This type of perturbation is of considerable practical importance in satellite design. Such time-dependent driving forces could arise from reciprocating masses, misaligned rotors with constant angular velocities, or rotors with time-dependent spin rates. In this paper, these torques are given the harmonic form $\varepsilon T_i \sin \Omega t$, where ε is a small perturbation parameter. The total momentum H and energy T of the body can be expressed as

$$H = (I_1\omega_1 + J\sigma_1)^2 + (I_2\omega_2 + J\sigma_2)^2 + (I_3\omega_3 + J\sigma_3)^2, \tag{2}$$

$$2T = (I_1 - J)\omega_1^2 + (I_2 - J)\omega_2^2 + (I_3 - J)\omega_3^2 + J[(\omega_1 + \sigma_1)^2 + (\omega_2 + \sigma_2)^2 + (\omega_3 + \sigma_3)^2]. \tag{3}$$

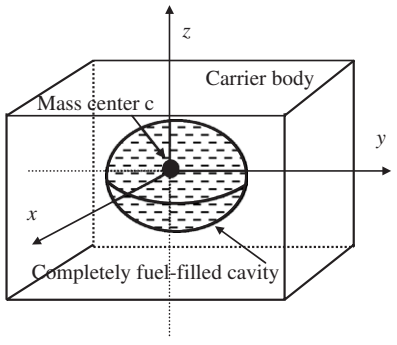

Fig. 1. Spacecraft model.

It is now convenient to make the equations of motion dimensionless and explicitly introduce the perturbation parameter ε. This will make it clearer which terms are of higher order in ε and therefore smaller, and which terms should be retained. We define the following dimensionless quantities:

$$\varepsilon \triangleq \frac{J}{I_2}, \qquad \tau = \frac{Ht}{I_2}, \qquad \tilde{H}_i = \frac{H_i}{H}, \qquad \tilde{H}_i' \triangleq \left(\frac{I_2}{H^2}\right)\dot{H}_i,$$
$$r_1 \triangleq \frac{I_3}{I_2} > 1, \qquad r_2 \triangleq \frac{I_1}{I_2} < 1, \quad \tilde{\mu} \triangleq \frac{\mu}{H} = O(\varepsilon), \quad \tilde{\sigma}_i \triangleq \frac{I_2}{\varepsilon H}\sigma_i,$$
$$\tilde{\sigma}_i' \triangleq \frac{I_2^2}{\varepsilon H^2}\dot{\sigma}_i, \quad \text{and} \quad \tilde{\Omega} \triangleq \frac{\Omega I_2}{H}.$$

The notation $()' = \mathrm{d}()/\mathrm{d}\tau$ denotes differentiation with respect to the dimensionless time τ, also defined above. We assume $I_1 < I_2 < I_3$, and therefore $0 < r_2 < 1 < r_1$. Note that the number of parameters describing the body moments of inertia has been reduced to two: $r_1 r_2$. Carrying out this change of variables leads to the equivalent set of dimensionless equations

$$\tilde{H}_1' = \frac{1 - r_1}{(r_1 - \varepsilon)(1 - \varepsilon)}\tilde{H}_2\tilde{H}_3 + \varepsilon(\tilde{\mu}\tilde{\sigma}_1 + T_1 \sin \tilde{\Omega}\tau), \tag{4a}$$

$$\tilde{H}_2' = \frac{r_1 - r_2}{(r_2 - \varepsilon)(r_1 - \varepsilon)}\tilde{H}_1\tilde{H}_3 + \varepsilon(\tilde{\mu}\tilde{\sigma}_2 + T_2 \sin \tilde{\Omega}\tau), \tag{4b}$$

$$\tilde{H}_3' = \frac{r_2 - 1}{(1 - \varepsilon)(r_2 - \varepsilon)}\tilde{H}_1\tilde{H}_2 + \varepsilon(\tilde{\mu}\tilde{\sigma}_3 + T_3 \sin \tilde{\Omega}\tau), \tag{4c}$$

$$\varepsilon\tilde{\sigma}_1' = \frac{\tilde{H}_3}{r_5 - 1}\tilde{\sigma}_2 - \frac{\tilde{H}_2}{r_4 - 1}\tilde{\sigma}_3 - \frac{\tilde{H}_1'}{r_2 - \varepsilon} - \tilde{\mu}\tilde{\sigma}_1, \tag{4d}$$

$$\varepsilon\tilde{\sigma}_2' = \frac{\tilde{H}_1}{r_3 - 1}\tilde{\sigma}_3 - \frac{\tilde{H}_3}{r_5 - 1}\tilde{\sigma}_1 - \frac{\tilde{H}_2'}{1 - \varepsilon} - \tilde{\mu}\tilde{\sigma}_2, \tag{4e}$$

$$\varepsilon\tilde{\sigma}_3' = \frac{\tilde{H}_2}{r_4 - 1}\tilde{\sigma}_1 - \frac{\tilde{H}_1}{r_3 - 1}\tilde{\sigma}_2 - \frac{\tilde{H}_3'}{r_1 - \varepsilon} - \tilde{\mu}\tilde{\sigma}_3, \tag{4f}$$

where $r_3 = I_1/J$, $r_4 = I_2/J$, and $r_5 = I_3/J$. Eqs. (4a)–(4f) are the full equations of motion, with no simplifying assumptions. As we shall see, in order to apply Melnikov's method these equations must now be separated into an unperturbed part plus a series of perturbed terms. This is done by expanding the equations in powers of ε; only terms up to the appropriate order in ε will be retained. To first order, the equations of motion can be written as

$$\tilde{H}_1' = \frac{1 - r_1}{r_1}\tilde{H}_2\tilde{H}_3 + \varepsilon\left(\left(\frac{1}{r_1^2} - 1\right)\tilde{H}_2\tilde{H}_3 + \tilde{\mu}\tilde{\sigma}_1 + T_1 \sin \tilde{\Omega}\tau\right) + O(\varepsilon^2), \tag{5a}$$

$$\tilde{H}_2' = \frac{r_1 - r_2}{r_2 r_1}\tilde{H}_1\tilde{H}_3 + \varepsilon\left(\left(\frac{1}{r_2^2} - \frac{1}{r_2^1}\right)\tilde{H}_1\tilde{H}_3 + \tilde{\mu}\tilde{\sigma}_2 + T_2 \sin \tilde{\Omega}\tau\right) + O(\varepsilon^2), \tag{5b}$$

$$\tilde{H}_3' = \frac{r_2 - 1}{r_2}\tilde{H}_1\tilde{H}_2 + \varepsilon\left(\left(1 - \frac{1}{r_2^2}\right)\tilde{H}_1\tilde{H}_2 + \tilde{\mu}\tilde{\sigma}_3 + T_3 \sin \tilde{\Omega}\tau\right) + O(\varepsilon^2), \tag{5c}$$

$$\varepsilon\tilde{\sigma}_1' = \frac{\tilde{H}_3}{r_5 - 1}\tilde{\sigma}_2 - \frac{\tilde{H}_2}{r_4 - 1}\tilde{\sigma}_3 - \frac{\tilde{H}_1'}{r_2} - \tilde{\mu}\tilde{\sigma}_1 + O(\varepsilon), \tag{5d}$$

$$\varepsilon\tilde{\sigma}_2' = \frac{\tilde{H}_1}{r_3 - 1}\tilde{\sigma}_3 - \frac{\tilde{H}_3}{r_5 - 1}\tilde{\sigma}_1 - \tilde{H}_2' - \tilde{\mu}\tilde{\sigma}_2 + O(\varepsilon), \tag{5e}$$

$$\varepsilon\tilde{\sigma}_3' = \frac{\tilde{H}_2}{r_4 - 1}\,\tilde{\sigma}_1 - \frac{\tilde{H}_1}{r_3 - 1}\,\tilde{\sigma}_2 - \frac{\tilde{H}_3'}{r_1} - \tilde{\mu}\tilde{\sigma}_3 + O(\varepsilon). \tag{5f}$$

In the next section, we describe a procedure that can reduce Eqs. (5a)–(5f) to three equations which have an unperturbed, spherical phase space, by the elimination of Eqs. (5d)–(5f). Due to the nature of this procedure, we do not need to retain any terms of $O(\varepsilon)$ or higher on the right-hand side of Eqs. (5d)–(5f).

2.2. Melnikov's method

To apply Melnikov's method, the unperturbed phase space must include heteroclinic orbits between pairs of saddle points and/or homoclinic orbits from a single saddle point. Melnikov's method will evaluate changes in the Poincaré map of the phase space when the system is perturbed. The unperturbed phase space for the system given in Eqs. (5a)–(5f) is of course found by setting $\varepsilon = 0$. Doing so eliminates the interdependence between Eqs. (5a)–(5c) and Eqs. (5d)–(5f) and allows us to solve Eqs. (5a)–(5c) independently. The unperturbed system of equations corresponding to Eqs. (5a)–(5c) is

$$\tilde{H}_1' = \frac{1 - r_1}{r_1}\,\tilde{H}_2\tilde{H}_3, \tag{6a}$$

$$\tilde{H}_2' = \frac{r_1 - r_2}{r_2 r_1}\,\tilde{H}_1\tilde{H}_3, \tag{6b}$$

$$\tilde{H}_3' = \frac{r_2 - 1}{r_2}\,\tilde{H}_1\tilde{H}_2. \tag{6c}$$

These equations are identical to Euler's rotational equations of motion for a torque-free rigid body. The spherical phase space for the unperturbed system is shown in Fig. 2, where the dimensionless, body-fixed angular momentum components $\tilde{H}_1, \tilde{H}_2, \tilde{H}_3$ are the phase variables. This phase space has six equilibrium points at $\{(\pm 1,0,0), (0,\pm 1,0), (0,0,\pm 1)\}$, where the equilibrium points $(\pm 1,0,0)$ and $(0,0,\pm 1)$ are neutrally stable centers corresponding to spin around the minor and major axis, respectively. The equilibrium points at $(0,\pm 1,0)$ are unstable, hyperbolic saddle points corresponding to spin about the intermediate axis. Note the presence of heteroclinic orbits joining the two saddle points.

Melnikov's method can now be applied to Eqs. (5a)–(5f). Melnikov's method is a perturbation technique that gives global information about the dynamics of the system. The method detects intersections of the stable and unstable hyperbolic saddle manifolds in planar Poincaré maps. The existence of these intersections implies the existence of Smale horseshoes and chaos, via the Smale-Birkhoff theorem [16]. For a detailed presentation of Melnikov's theory, see the work of Wiggins, or of Guckenheimer and Holmes [17,18]. The most common version of Melnikov's method considers systems of the form

$$x = f(x;\mu) + \varepsilon g(x,\tau;\mu), \quad x = \begin{Bmatrix} u \\ v \end{Bmatrix} \in R^2, \tag{7}$$

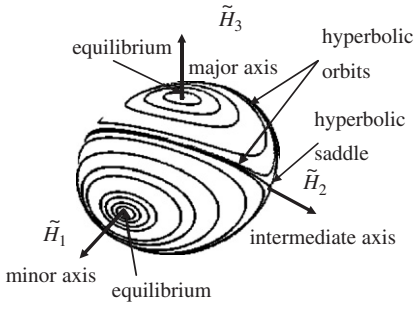

Fig. 2. Momentum sphere illustrating the heteroclinic orbits and the hyperbolic saddle points; curves are orbits of constant energy.

where g is periodic in τ, $f(x)$ is a Hamiltonian vector field defined on R^2, and $\varepsilon g(x, \tau)$ is a small perturbation which need not be Hamiltonian. It would appear that Melnikov's method is not applicable to our system, given the form of Eq. (7). While Melnikov's method applies to systems whose Poincaré map is planar, the system considered here is six dimensional. On the other hand, close inspection of Eqs. (5a)–(5f) reveals that Eqs. (5d)–(5f) couple with Eqs. (5a)–(5c) only through the perturbation terms in Eqs. (5a)–(5c). We therefore first find the unperturbed solutions of Eqs. (5a)–(5c) (i.e., $\tilde{H}_1, \tilde{H}_2, \tilde{H}_3$ in the case $\varepsilon = 0$), then substitute these solutions into Eqs. (5d)–(5f). We then solve Eqs. (5d)–(5f) for *their* unperturbed solutions (σ_1, σ_2, σ_3 in the case $\varepsilon = 0$), and substitute the resulting formulas for σ_1, σ_2, σ_3 back into the perturbation terms of Eqs. (5a)–(5c). This process results in three interdependent equations for $\tilde{H}_1, \tilde{H}_2, \tilde{H}_3$, where the unperturbed terms just represent Euler's equations of rotational motion and the perturbation terms depend on the $\tilde{H}_i$, the system parameters, and the dimensionless time τ. This process reduces our system from six to three first-order equations, but still does not allow us to use the planar form of Melnikov's method. However, a result due to Holmes and Marsden [15] does allow us to apply Melnikov's method directly to the equations involving $\tilde{H}_1, \tilde{H}_2, \tilde{H}_3$. The Melnikov function [15] can be written in the form

$$M(\tau_0) = \int_{-\infty}^{\infty} \nabla\tilde{H}[q_0(\tau)]\{f[q_0(\tau)] + g[q_0(\tau), \tau + \tau_0]\}\,\mathrm{d}\tau, \tag{8}$$

where $\nabla\tilde{H}$ is the gradient with respect to $\tilde{H}_i$ of the unperturbed system Hamiltonian $\tilde{H}$, f is the unperturbed part of the system equations, g is the $O(\varepsilon)$ perturbation of the system equations, and $q_0(\tau)$ is the solution of a heteroclinic orbit or trajectory of the unperturbed system. The dimensionless Hamiltonian of the system is given by $\tilde{H} = \frac{1}{2}(\tilde{H}_1^2/r_2 + \tilde{H}_2^2 + \tilde{H}_3^2/r_1)$, and is simply the kinetic energy of the unperturbed system (i.e., the carrier body). The gradient of $\tilde{H}$ with respect to the body-fixed angular momentum components is thus the vector $\nabla\tilde{H} = \{\tilde{H}_1/r_2,\ \tilde{H}_2,\ \tilde{H}_3/r_1\}$. Because it can be readily shown that $\nabla\tilde{H}f = 0$, Eq. (8) simplifies to

$$M(\tau_0) = \int_{-\infty}^{\infty} \nabla\tilde{H}[q_0(\tau)]g[q_0(\tau), \tau + \tau_0]\,\mathrm{d}\tau. \tag{9}$$

Before this integral can be evaluated, we must find the heteroclinic orbits q_0 of the unperturbed system given by Eqs. (6a)–(6c). Then we must find the unperturbed solutions to Eqs. (5d)–(5f), so that we can substitute for $\tilde{\sigma}_i$ in the perturbation terms of Eqs. (5a)–(5c).

Solutions for the heteroclinic orbits can be readily found in terms of hyperbolic trigonometric functions [1]. These solutions are as follows:

$$\tilde{H}_1 = s_1 X_1 \operatorname{sech}(D\tau), \tag{10a}$$

$$\tilde{H}_2 = s_2 \tanh(D\tau), \tag{10b}$$

$$\tilde{H}_3 = s_3 X_3 \operatorname{sech}(D\tau), \tag{10c}$$

where $X_1 \triangleq \sqrt{r_2(1-r_1)/(r_2-r_1)}$, $X_3 \triangleq \sqrt{r_1(r_2-1)/(r_2-1)}$, and $D \triangleq \sqrt{(r_1-1)(1-r_2)/(r_1 r_2)}$. The signs $\{s_1, s_2, s_3\} = \pm 1$ must be chosen such that the product $s_1 s_2 s_3 = 1$; these permutations give rise to all four of the heteroclinic orbits shown in Fig. 2.

We can solve Eqs. (5d)–(5f) (with $\varepsilon = 0$) for $\tilde{\sigma}_i$ by substituting in the unperturbed solutions for $\tilde{H}_i$ and $\tilde{H}_i'$. The approximate solutions to these equations are

$$\tilde{\sigma}_1 = -\frac{1}{\tilde{\mu}}\left[\frac{\tilde{H}_1'}{r_2} - \frac{\tilde{H}_3}{r_5 - 1}\tilde{\sigma}_2 + \frac{\tilde{H}_2}{r_4 - 1}\tilde{\sigma}_3\right], \tag{11a}$$

$$\tilde{\sigma}_2 = \frac{-((\tilde{H}_3\tilde{H}_1'/(r_5-1)r_2) + \tilde{\mu}\tilde{H}_2' - [((\tilde{H}_3\tilde{H}_2^2)/(r_5-1)(r_4-1)) + (\tilde{\mu}\tilde{H}_1/(r_4-1))]\tilde{\sigma}_3}{-((\tilde{H}_2^2)/(r_5-1)^2)}, \tag{11b}$$

$$\tilde{\sigma}_3 = \frac{((\tilde{H}_3\tilde{H}_1\tilde{H}_1')/((r_5-1)(r_3-1)r_2)) - ((\tilde{H}_3\tilde{H}_2\tilde{H}_2')/((r_4-1)(r_5-1))) - ((\tilde{H}_3^2\tilde{H}_3')/((r_5-1)^2 r_1))}{\tilde{\mu}((\tilde{H}_1)/(r_3-1))^2 + \tilde{\mu}((\tilde{H}_2)/(r_4-1))^2 + \tilde{\mu}((\tilde{H}_3)/(r_5-1))^2}. \tag{11c}$$

In accordance with Melnikov's method, we now replace τ by $\tau+\tau_0$ everywhere that τ appears explicitly. We then substitute the resulting expression for $\tilde{\sigma}_i$ into Eqs. (5a)–(5c), to obtain the final form of the Melnikov integral.

2.3. Melnikov's function

The Melnikov integral given in Eq. (9) can now be expanded, where $\tilde{H}_1, \tilde{H}_2, \tilde{H}_3$ are the unperturbed solutions equations (10a)–(10c) along the heteroclinic orbits. Because the range of the integral is $(-\infty, +\infty)$, all odd functions in the integrand can be eliminated. This leaves the following terms:

$$M(\tau_0) = \int_{-\infty}^{\infty} \frac{2\tilde{H}_1}{r_2}\tilde{\mu}\tilde{\sigma}_1\,\mathrm{d}\tau + \int_{-\infty}^{\infty} \frac{2\tilde{H}_1}{r_2} T_1\,\cos(\tilde{\Omega}\tau)\sin(\tilde{\Omega}\tau_0)\,\mathrm{d}\tau + \int_{-\infty}^{\infty} 2\tilde{H}_2\tilde{\mu}\,\tilde{\sigma}_2\,\mathrm{d}\tau + \int_{-\infty}^{\infty} 2\tilde{H}_2 T_2\,\sin(\tilde{\Omega}\tau)\cos(\tilde{\Omega}\tau_0)\,\mathrm{d}\tau + \int_{-\infty}^{\infty} \frac{2\tilde{H}_3}{r_1}\cos(\tilde{\Omega}\tau)\sin(\Omega\tau_0)\,\mathrm{d}\tau. \tag{12}$$

Let us define

$$A_1 = \int_{-\infty}^{\infty} \frac{2\tilde{H}_1}{r_2}\tilde{\mu}\tilde{\sigma}_1\,\mathrm{d}\tau, \tag{13}$$

$$B_1 = \int_{-\infty}^{\infty} \frac{2\tilde{H}_1}{r_2} T_1\,\cos(\tilde{\Omega}\tau)\,\mathrm{d}\tau, \tag{14}$$

$$A_2 = \int_{-\infty}^{\infty} 2\tilde{H}_2\tilde{\mu}\tilde{\sigma}_2\,\mathrm{d}\tau, \tag{15}$$

$$B_2 = \int_{-\infty}^{\infty} 2\tilde{H}_2 T_2\,\sin(\tilde{\Omega}\tau)\,\mathrm{d}\tau, \tag{16}$$

$$C = \int_{-\infty}^{\infty} \frac{2\tilde{H}_3}{r_1}\cos(\tilde{\Omega}\tau)\,\mathrm{d}\tau. \tag{17}$$

Substituting the terms defined in expressions (10) and (11), one obtains

$$A_1 = \int_{-\infty}^{\infty} \frac{2\tilde{H}_1}{r_2}\tilde{\mu}\tilde{\sigma}_1\,\mathrm{d}\tau = \int_{-\infty}^{\infty} \frac{2\tilde{\mu}(r_6-1)X_1}{r_2 X_3}[\mathrm{sech}(D\tau)]^2\,\mathrm{d}\tau + \int_{-\infty}^{\infty} \frac{F[\sinh(D\tau)]^2}{[\cosh(D\tau)]^4\{p_1+p_2[\sinh(D\tau)]^2\}}\mathrm{d}\tau = A_{10}+A_{11}, \tag{18}$$

$$B_1 = \int_{-\infty}^{\infty} \frac{2X_1T_1}{r_2}\mathrm{sech}(D\tau)\cos(\tilde{\Omega}\tau)\,\mathrm{d}\tau, \tag{19}$$

$$A_2 = -\frac{2\tilde{\mu}(r_5-1)X_1 D}{r_2 X_3}\int_{-\infty}^{\infty} \frac{[\mathrm{sech}(D\tau)]^2}{[\mathrm{csch}(D\tau)]^2}\,\mathrm{d}\tau, \tag{20}$$

$$B_2 = \int_{-\infty}^{\infty} 2T_2\,\tanh(D\tau)\sin(\Omega\tau)\,\mathrm{d}\tau, \tag{21}$$

$$C = \int_{-\infty}^{\infty} \frac{2X_3T_3}{r_1}\mathrm{sech}(D\tau)\cos(\tilde{\Omega}\tau)\,d\tau. \tag{22}$$

Eq. (18) makes use of the additional terms

$$F = \frac{1}{\tilde{\mu}}\left[\frac{2DX_3X_1^3}{r_2^2(r_5-1)(r_4-1)(r_3-1)} + \frac{2DX_3X_1}{r_2(r_5-1)(r_4-1)^2} - \frac{2DX_3^3X_1}{r_1r_2(r_5-1)^2(r_4-1)}\right], \tag{23}$$

$$p_1 = \left(\frac{X_1}{r_3 - 1}\right)^2 + \left(\frac{X_3}{r_5 - 1}\right)^2, \tag{24}$$

$$p_2 = \left(\frac{1}{r_4 - 1}\right)^2, \tag{25}$$

$$A_{10} = \int_{-\infty}^{\infty} \frac{2\tilde{\mu}(r_6 - 1)X_1}{r_2 X_3} [\mathrm{sech}(D\tau)]^2 \, \mathrm{d}\tau, \tag{26}$$

$$A_{11} = \int_{-\infty}^{\infty} \frac{F[\sinh(D\tau)]^2}{[\cosh(D\tau)]^4 \{p_1 + p_2[\sinh(D\tau)]^2\}} \, \mathrm{d}\tau. \tag{27}$$

By manipulating these equations symbolically with Mathematica 4, we obtain the solutions

$$A_{10} = \int_{-\infty}^{\infty} \frac{2\tilde{\mu}(r_5 - 1)X_1}{r_2 X_3} [\mathrm{sech}(D\tau)]^2 \, \mathrm{d}\tau = \frac{4\tilde{\mu}(r_5 - 1)X_1}{r_2 X_3}, \tag{28}$$

$$B_1 = \int_{-\infty}^{\infty} \frac{2X_1 T_1}{r_2} \mathrm{sech}(D\tau) \cos(\tilde{\Omega}\tau) \, \mathrm{d}\tau = \frac{X_1 T_1 \, \mathrm{sech}(\tilde{\Omega}\pi/2D)}{r_2 D}, \tag{29}$$

$$A_2 = -\frac{2\tilde{\mu}(r_5 - 1)X_1 D}{r_2 X_3} \int_{-\infty}^{\infty} \frac{[\mathrm{sech}(D\tau)]^2}{[\mathrm{csch}(D\tau)]^2} \, \mathrm{d}\tau = -\frac{4\tilde{\mu}(r_5 - 1)X_1}{r_2 X_3}, \tag{30}$$

$$B_2 = \int_{-\infty}^{\infty} 2T_2 \, \tanh(D\tau) \sin(\Omega\tau) \, \mathrm{d}\tau = -\frac{T_2 \pi \, \mathrm{csch}(\tilde{\Omega}\pi/4D)\mathrm{sech}(\tilde{\Omega}\pi/4D)}{D}, \tag{31}$$

$$C = \int_{-\infty}^{\infty} \frac{2X_3 T_3}{r_1} \mathrm{sech}(D\tau) \cos(\tilde{\Omega}\tau) \, \mathrm{d}\tau = \frac{2T_3 X_3 \pi \, \mathrm{sech}(\tilde{\Omega}\pi/2D)}{r_1 D}. \tag{32}$$

Integral (27) can be evaluated via residue theory (see Appendix A for details), yielding

$$\begin{aligned} A_{11} = & \int_{-\infty}^{\infty} \frac{F[\sinh(D\tau)]^2}{[\cosh(D\tau)]^4 \{p_1 + p_2[\sinh(D\tau)]^2\}} \mathrm{d}\tau \\ & \times \underline{\underline{(D\tau = z)}} \, F_0 \left\{ 2 \lim_{z \to a} \frac{1}{3!} \frac{\mathrm{d}^3}{\mathrm{d}z^3} \left[(z - a)^4 \frac{f(z)}{h(z)} \right] + 2 \lim_{z \to b} \frac{\mathrm{d}}{\mathrm{d}z} \left[(z - b) \frac{f(z)}{h(z)} \right] \right\} \\ = & \, 2F_0(M_{a_1} + M_{a_2}). \end{aligned} \tag{33}$$

In this solution, we have defined the terms

$$F_0 = \frac{1}{\tilde{\mu}} \cdot \left[\frac{2X_3 X_1^3}{r_2^2 (r_5 - 1)(r_4 - 1)(r_3 - 1)} + \frac{2X_3 X_1}{r_2 (r_5 - 1)(r_4 - 1)^2} - \frac{2X_3^3 X_1}{r_1 r_2 (r_5 - 1)^2 (r_4 - 1)} \right], \tag{34}$$

$$M_{a_1} = \lim_{z \to a} \frac{1}{3!} \frac{\mathrm{d}^3}{\mathrm{d}z^3} \left[(z - a_1)^4 \frac{f(z)}{h(z)} \right], \tag{35}$$

$$M_{a_2} = \lim_{z \to b} \frac{\mathrm{d}}{\mathrm{d}z} \left[(z - a_2) \frac{f(z)}{h(z)} \right], \tag{36}$$

$$f(z) = \left(\frac{\pi}{2} i - z \right) [\sinh(z)]^2, \tag{37}$$

$$h(z) = [\cosh \, z(z)]^4 \{p_1 + p_2[\sinh(z)]^2\}, \tag{38}$$

where $a_1 = (\pi/2)i$ is the fourth-order pole and $a_2 = \arcsin \sqrt{(p_1/p_2)}i$ is the first-order pole of the integrand. Ofcourse, i is the imaginary unit.

Substituting Eqs. (28)–(33) into Eq. (12), we arrive at the Melnikov function for our system of equations:

$$M(\tau_0) = F_0(M_a + M_b) + \sqrt{(B_1 + C)^2 + B_2^2}\,\sin(\tilde{\Omega}\tau_0 + \varphi), \tag{39}$$

where $\varphi = \text{arc}tg((B_1 + C)/B_2)$. The Melnikov criterion is thus

$$\sqrt{(B_1 + C)^2 + B_2^2} > F_0(M_a + M_b). \tag{40}$$

Close inspection of Eq. (40) reveals that since $F_0 = F_0(r_1, r_2, r_3, r_4, r_5, \tilde{\mu})$, $B_1 = B_1(r_1, r_2, \tilde{\Omega}, T_1)$, $B_2 = B_2(r_1, r_2, \tilde{\Omega}, T_2)$, and $C = C(r_1, r_2, \tilde{\Omega}, T_3)$, Eq. (40) is a function of the ten system parameters $r_1, r_2, r_3, r_4, r_5, \tilde{\mu}, \tilde{\Omega}, T_1, T_2, T_3$. If condition (40) is satisfied, then the system modeled by Eqs. (5a)–(5f) will exhibit chaotic dynamics near the heteroclinic orbits for sufficiently small ε.

3. Results based on Melnikov's method

We have analytically proven the existence of chaotic evolution in the attitude of an energy-dissipating, liquid-filled satellite subject to time-periodic perturbations. Criterion (40) can be used to separate the chaotic and non-chaotic regions of parameter space, and if necessary avoid chaotic motion in this class of satellites. The Melnikov chaos criterion depends on ten parameters: the dimensionless moments of inertia r_1, r_2, the fuel slug parameters r_3, r_4, r_5, the driving frequency of the perturbing torques $\tilde{\Omega}$, the amplitudes of the perturbing torques T_1, T_2, T_3, and the damping parameter $\tilde{\mu}$. By fixing seven of these parameters, the remaining three-dimensional parameter space can be studied in detail. Some of these three-dimensional studies are shown in Figs. 3–5.

Fig. 3 shows the dividing surface between chaotic and non-chaotic motion in the $\tilde{\Omega} - T_1 - \tilde{\mu}$ space, as determined by Eq. (40). The moment of inertia parameters were set to $r_1 = 1.3$, $r_2 = 0.2$, $r_3 = 55.6$, $r_4 = 83.2$, $r_5 = 111.2$. Parameter values above the surface shown lead to chaotic motion. The surface flattens at $\tilde{\mu} = 1$ because we have imposed the condition $\tilde{u} < 1$. We can see that as T_1 increases, chaotic motion becomes easier to achieve. For sufficiently small T_1, on the other hand, it is impossible to obtain chaotic motion. Fig. 4 shows the dividing surface between chaotic and non-chaotic motion in the $r_1 - T_1 - \tilde{\mu}$ space, as determined by Eq. (40). The surface shows the extent to which chaotic motion depends on the shape of the rigid body. We see that as $r_1 \to 1$, the value corresponding to a nearly symmetric, prolate body, we enter a region where no chaotic motion occurs. Fig. 5 also shows the dependence of chaotic motion on the shape of the rigid body, but this time for r_2 instead of r_1. We see that as $r_2 \to 1$, chaotic motion becomes impossible for any value of T_1. This shape corresponds to a nearly symmetric, oblate carrier body.

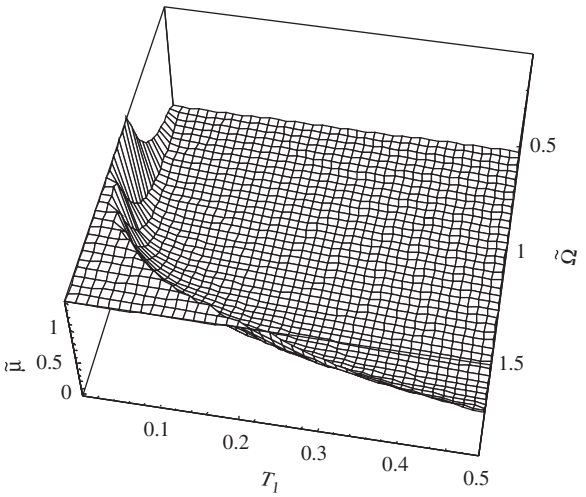

Fig. 3. The surface separating chaotic from non-chaotic for the parameter space $\tilde{\Omega} - T_1 - \tilde{\mu}$.

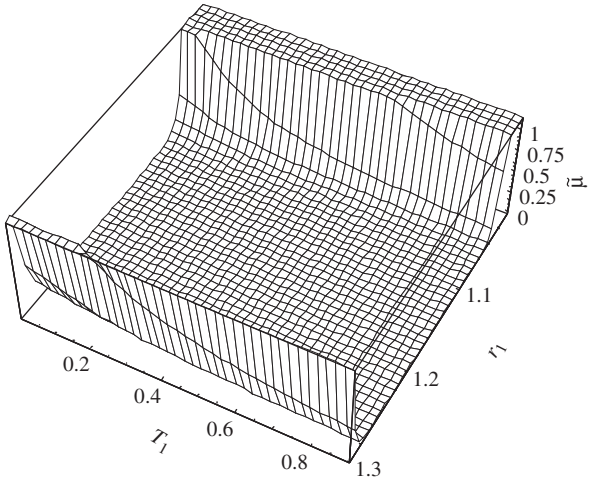

Fig. 4. The surface separating chaotic from non-chaotic motion for the parameter space $r_1 - T_1 - \tilde{\mu}$.

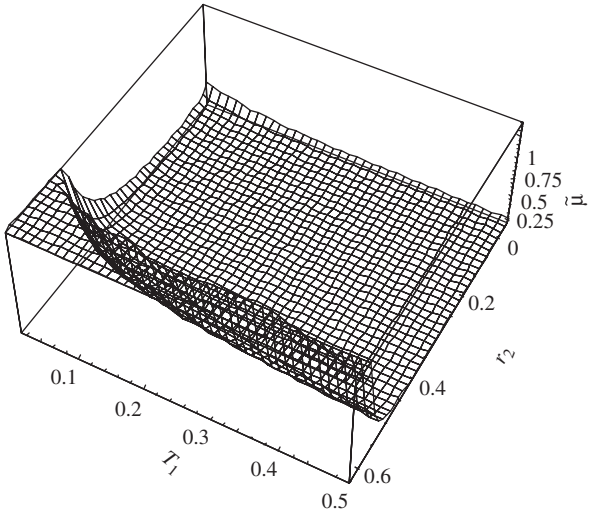

Fig. 5. The surface separating chaotic from non-chaotic motion for the parameter space $r_2 - T_1 - \tilde{\mu}$.

4. Numerical simulation

In the case of zero external driving torque ($T_i = 0$), the viscous fuel slug dissipates energy. Over time, T decreases and the energy ellipsoid shrinks. As shown in Figs. 6 and 7, this leads to an open polhode path that spirals outward from the minor axis and is captured at one of the major axes. Fig. 6 was obtained by numerically solving Eqs. (5) with the following initial conditions and parameters:

$$(\cos(pi/36), -\sin(pi/36), 0.0001, 0, 0, 0.2), \quad r_1 = 1.3, \quad r_2 = 0.67.$$

Fig. 7 was obtained by simulating Eqs. (5) with the following initial conditions and parameters:

$$(\cos(pi/36), -\sin(pi/36), 0.0001, 0, 0, -0.2), \quad r_1 = 1.3, \quad r_2 = 0.67.$$

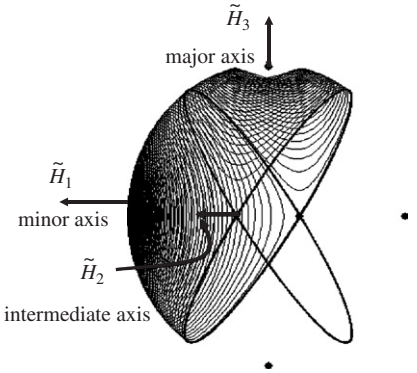

Fig. 6. The path of the angular velocity vector in body axis coordinates starts with a positive minor axis spin and finishes with positive major axis spin.

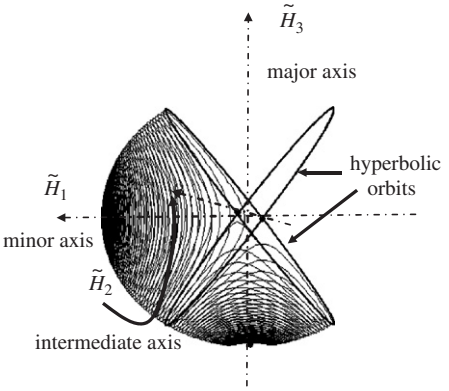

Fig. 7. The path of the angular velocity vector in body axis coordinates starts with a positive minor axis spin and finishes with negative major axis spin.

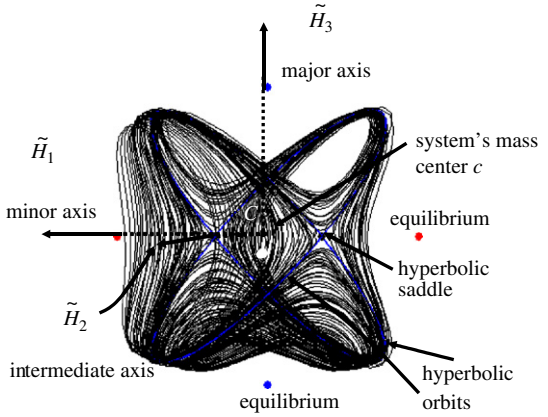

Fig. 8. The path of the angular velocity vector in body axis coordinates starts with a positive minor axis spin and finishes with chaotic spin.

As is clearly shown in Figs. 6 and 7, the orientation of the spacecraft relative to the fixed angular momentum vector at the end of the maneuver cannot be determined a priori. The spacecraft could end up with either a positive or a negative major axis spin. Physically, this corresponds to two final attitudes that are 180° apart.

In the presence of external perturbations, the spacecraft exhibits non-periodic solutions which possess many of the characteristics of randomness. Fig. 8 is obtained by simulating Eqs. (5) with the following initial conditions and parameters:

$$(\cos(pi/36), -\sin(pi/36), 0.5, 0, 0, 0.2),$$
$$r_1 = 1.39,\ \ r_2 = 0.45,\ \ \varepsilon = 0.013,\ \ T_1 = 0.001,\ \ T_2 = 0.001,\ \ T_3 = 0.001.$$

5. Concluding remarks

This paper derives the six-dimensional ordinary differential equations governing the attitude motion of a spacecraft with a completely liquid-filled cavity, subject to time-periodic perturbing torques. This system of equations is then transformed into a form suitable for the application of Melnikov's method. Using the Melnikov integral, we obtain a theoretical criterion for chaotic motion in the spacecraft's attitude. In addition, three-dimensional subspaces of the full nine-dimensional parameter space are studied analytically to obtain a qualitative and quantitative understanding of the interactions leading to nonlinear motion. An analysis of these results shows that the shape of the rigid body and the driving frequency of the perturbations have a profound influence on the appearance of chaotic dynamics. Numerical solutions to these equations show that the motion of a perturbed satellite possesses characteristics common to random, non-periodic solutions. This solution was also theoretically proven to be chaotic using Melnikov's method.

Acknowledgments

The authors gratefully acknowledge funding by the Natural Science Foundation of China (10272022, 10572022), and the Beijing Institute of Technology (000Y07). The author also would like to thank Prof. A. Doelman for his valuable help and Center for Mathematics and Computer Science (CWI) for the use of the computational facilities.

Appendix A. Evaluation of the Melnikov integral

Using an idea suggested by Or [5], we apply residue theory to the Melnikov integral. First one constructs a closed circuit C containing the two poles $z = a_1$ and a_2. In this case, we choose a rectangular strip in the upper half of the complex plane. C runs counter-clockwise through the points $z = -R$, $z = R$, $z = R+i\pi$, and $z = -R+i\pi$, and finally back to $z = -R$. By letting $R \to \infty$ and applying the residue theorem, we obtain

$$\begin{aligned} A_{11} &= \int_{-\infty}^{\infty} \frac{F[\sinh(D\tau)]^2}{[\cosh(D\tau)]^4\{p_1 + p[\sinh(D\tau)]^2\}}\,\mathrm{d}\tau = F_0\frac{1}{\pi i}\oint_C \frac{f(z)}{h(z)}\,\mathrm{d}z \\ &= F_0\frac{2\pi i}{\pi i}\left[\sum_{i=1}^{2}\operatorname*{Re}_{z=a_k} s\left(\frac{f(z)}{h(z)}\right)\right] \\ &= 2F_0(M_{a_1} + M_{a_2}). \end{aligned} \tag{A.1}$$

Expanding $f(z)$ and $h(z)$ into Taylor series around the point z_0, one obtains

$$f(z) = f_0(z_0) + f_1(z_0)(z - z_0) + \tfrac{1}{2}f_2(z_0)(z - z_0)^2 + \tfrac{1}{6}f_3(z_0)(z - z_0)^3 + \cdots, \tag{A.2}$$

$$\begin{aligned} h(z) = {} & h_0(z_0) + h_1(z_0)(z - z_0) + \tfrac{1}{2}h_2(z_0)(z - z_0)^2 \\ & + \tfrac{1}{6}h_3(z_0)(z - z_0)^3 + \tfrac{1}{24}h_4(z_0)(z - z_0)^4 \\ & + \tfrac{1}{120}h_5(z_0)(z - z_0)^5 + \tfrac{1}{720}h_6(z_0)(z - z_0)^6 + \cdots. \end{aligned} \tag{A.3}$$

If $z_0 = a_1$, then $h_0 = h(a_1) = 0$, $h_1 = (\mathrm{d}h/\mathrm{d}z)(a_1) = 0$, $h_2 = (\mathrm{d}^2h/\mathrm{d}z^2)(a_1) = 0$, and $h_3 = (\mathrm{d}^3h/\mathrm{d}z^3)(a_1) = 0$. The more interesting terms are

$$\begin{aligned} h_4 = \frac{\mathrm{d}^4h}{\mathrm{d}z^4}(a_1) &= 128p_2[\cosh z(a_1)]^4[\sinh(a_1)]^2 + p_2[\cosh(a_1)]^4\{8[\cosh(a_1)]^2 \\ &+ 8[\sinh(a_1)]^2\} + 6p_2\{2[\cosh(a_1)]^2 + 2[\sinh(a_1)]^2\}\{4[\cosh(a_1)]^4 \\ &+ 12[\cosh(a_1)]^2[\sinh(a_1)]^2\} + 8p_2\cosh(a_1)\sinh(a_1)\{40[\cosh(a_1)]^3\sinh(a_1) \\ &+ 24\cosh(a_1)[\sinh(a_1)]^3\} + \{p_1 + p_2[\sinh(a_1)]^2\}\{40[\cosh(a_1)]^4 \\ &+ 192[\cosh(a_1)]^2[\sinh(a_1)]^2 + 8[\sinh(a_1)]^2\}, \end{aligned}$$

$$\begin{aligned} h_5 = \frac{\mathrm{d}^5h}{\mathrm{d}z^5}(a_1) &= 32p_2[\cosh z(a_1)]^5\sinh(a_1) + 20p_2[\cosh(a_1)]^3\sinh(a_1)\{8[\cosh(a_1)]^2 + 8[\sinh(a_1)]^2\} \\ &+ 80p_2\cosh(a_1)\sinh(a_1)\{4[\cosh(a_1)]^4 + 12[\cosh(a_1)]^2[\sinh(a_1)]^2\} + 10p_2\{2[\cosh(a_1)]^2 + 2[\sinh(a_1)]^2\} \\ &\times \{40[\cosh(a_1)]^3\sinh(a_1) + 24\cosh(a_1)[\sinh(a_1)]^3\} + \{p_1 + p_2[\sinh(a_1)]^2\}\{544[\cosh(a_1)]^3\sinh(a_1) \\ &+ 480\cosh(a_1)[\sinh(a_1)]^3\} + 10p_2\cosh(a_1)\sinh(a_1)\{40[sosh(a_1)]^4 \\ &+ 192[\cosh(a_1)]^2[\sinh(a_1)]^2 + 24[\sinh(a_1)]^4\} \end{aligned}$$

and

$$\begin{aligned} h_6 = \frac{\mathrm{d}^6h}{\mathrm{d}z^6}(a_1) &= 768p_2[\cosh z(a_1)]^4[\sinh(a_1)]^2 + p_2[\cosh(a_1)]^4\{32[\cosh(a_1)]^2 + 32[\sinh(a_1)]^2\} \\ &+ 15p_2\{8[\cosh(a_1)]^2 + 8[\sinh(a_1)]^2\}\{4[\cosh(a_1)]^4 + 12[\cosh(a_1)]^2[\sinh(a_1)]^2\} + 160p_2\cosh(a_1) \\ &\times \sinh(a_1)\{40[\cosh(a_1)]^3\sinh(a_1) + 24\cosh(a_1)[\sinh(a_1)]^3\} + 12p_2\cosh(a_1)\sinh(a_1)\{544[\cosh(a_1)]^3 \\ &\times \sinh(a_1) + 480\cosh(a_1)[\sinh(a_1)]^3\} + 15p_2\{[\cosh(a_1)]^2 + 2[\sinh(a_1)]^2\}\{40[\cosh(a_1)]^4 + 192[\cosh(a_1)]^2 \\ &\times [\sinh(a_1)]^2 + 24[\sinh(a_1)]^4\} + \{p_1 + p_2[\sinh(a_1)]^2\}\{544[\cosh(a_1)]^4 \\ &+ 3072[\cosh(a_1)]^2[\sinh(a_1)]^2 + 480[\sinh(a_1)]^4\}. \end{aligned}$$

For $z_0 = a_1$ we also have

$$\begin{aligned} &f_0 = 0,\ f_1 = [\sinh(a_1)]^2,\ f_2 = -4\sinh(a_1)\cosh(a_1) \text{ and} \\ &f_3 = -4[\sinh(a_1)]^2 - 4\{[\sinh(a_1)]^2 + [\cosh(a_1)]^2\}. \end{aligned}$$

M_{a_1} can thus be evaluated via residue theory as

$$M_{a_1} = \frac{4}{h_4}\left[\frac{f_3}{6} - \frac{h_6}{30h_4} - \frac{h_5}{5h_4}\left(\frac{f_2}{2} - \frac{h_5f_1}{5h_4}\right)\right]. \tag{A.4}$$

If $z_0 = a_2$, then we have $h_0 = h(a_2) = 0$,

$$h_1 = \frac{\mathrm{d}h}{\mathrm{d}z}(a_2) = 2p_2[\cosh(a_2)]^5\sinh(a_2) + 4[\cosh(a_2)]^3\sinh(a_2)\{p_1 + p_2[\sinh(a_2)]^2\}$$

and

$$f_0 = \left(\frac{\pi}{2}i - a_2\right)[\sinh(a_2)]^2.$$

M_{a_2} can thus be evaluated via residue theory as

$$M_{a_2} = \frac{f_0}{h_1}. \tag{A.5}$$

Substituting (4) and (5) into (1) yields the result

$$A_{11} = 2F_0 \left\{ \frac{4}{h_4} \left[\frac{f_3}{6} - \frac{h_6}{30h_4} - \frac{h_5}{5h_4} \left(\frac{f_2}{2} - \frac{h_5 f_1}{5h_4} \right) \right] \Big|_{z=a_1} + \frac{f_0}{h_1} \Big|_{z=a_2} \right\}. \tag{A.6}$$

References

[1] G.J. Adams, Dual-spin spacecraft dynamics during platform spin-up, *Journal of Guidance and Control* 3 (1980) 29–36.

[2] J.E. Cochran, H.E. Hkolloway, Resonance in the attitude motions of asymmetric dual-spin spacecraft, *Journal of the Astronautical Sciences* 28 (1980) 231–254.

[3] J.R. Gebman, D.L. Mingori, Perturbation solution for the flat spin recovery of a dual-spin spacecraft, *AIAA Journal* 14 (1976) 859–867.

[4] C.D. Hall, R.H. Rand, Spin-up dynamics of axial dual-spin spacecraft, *Journal of Guidance, Control, and Dynamics* 17 (1994) 30–37.

[5] A.C. Or, Resonances in the design dynamics of dual-spin spacecraft, *Journal of Guidance, Control, and Dynamics* 14 (1991) 321–329.

[6] P.M. Barba, N. Furumoto, I.P. Leliakov, Techniques for flat-spin recovery of spinning satellites, *AIAA Guidance and Control Conference, Key Biscayine, Florida, AIAA Paper*, 1973, pp. 73–859.

[7] V.V. Rumyantsev, On the Lyapunov's methods in the study of stability of motions of rigid bodies with fluid-filled cavities, *Advances in Applied Mechanics* 8 (1964) 183–232.

[8] D.R. Christopher, Reorientation maneuver for spinning spacecraft, *Journal of Guidance, Control, and Dynamics* 14 (1991) 724–728.

[9] G.L. Gray, L. Dobson, D.C. Kammer, Chaos in a spacecraft attitude maneuver due to time-periodic perturbations, *Journal of Applied Mechanics* 63 (1996) 501–508.

[10] A.J. Miller, G.L. Gray, Nonlinear spacecraft dynamics with a flexible appendage damping, and moving internal sub-masses, *Journal of Guidance, Control, and Dynamics* 24 (2001) 605–615.

[11] X. Tong, B. Tabarrok, Bifurcation of self-excited rigid bodies subjected to small perturbation torques, *Journal of Guidance, Control, and Dynamics* 20 (1997) 123–128.

[12] J.H. Cooper, R.H. Bishop, Chaos in rigid body attitude dynamics, *AIAA Paper* (1999) 99–3970.

[13] P.A. Meehan, S.F. Asokanthan, in: W.H. Kliemann, W.F. Alangford, N.S. Namachchivaya (Eds.), *Chaotic Motion in a Rotating Body with Internal Energy Dissipation, Nonlinear Dynamics and Stochastic Mechanics*, American Mathematical Society, Providence, RI, 1996, pp. 175–205.

[14] P.A. Meehan, S.F. Asokanthan, Control of chaotic motion in a spinning spacecraft with a circumferential nutation damper, *Nonlinear Dynamics* 17 (1998) 269–284.

[15] P.J. Holmes, J.E. Marsden, Horseshoes and Arnold diffusion for Hamiltonian systems on Lie groups, *Indiana University Mathematics Journal* 32 (1989) 273–309.

[16] J. Guckenheimer, P. Holmes, *Nonlinear Oscillations, Dynamical Systems, and Bifurcations of Vector Fields*, Springer, New York, 1983.

[17] S. Wiggins, *Global Bifurcations and Chaos*, Springer, New York, 1998.

[18] S. Wiggins, *Introduction to Applied Nonlinear Dynamics Systems and Chaos*, Springer, New York, 1990.